Chemical bonding and the role of node-induced electron confinement

Alistair J. Sterling,[†,‡] Daniel S. Levine,[†] Abdulrahman Aldossary,[†,¶] and Martin Head-Gordon[*,†,‡]

†*Pitzer Center for Theoretical Chemistry, Department of Chemistry, University of California, Berkeley, CA 94720, United States*

‡*Chemical Sciences Division, Lawrence Berkeley National Laboratory, Berkeley, CA 94720, United States*

¶*Current address: Department of Chemistry, University of Toronto, Toronto, Ontario, M5S 3H6, Canada*

E-mail: mhg@cchem.berkeley.edu

Abstract

The chemical bond is the cornerstone of chemistry, providing a conceptual framework to understand and predict the behavior of molecules in complex systems. However, the fundamental origin of chemical bonding remains controversial, and has been responsible for fierce debate over the past century. Here we present a unified theory of bonding, using a separation of electron delocalization effects from orbital relaxation to identify three mechanisms – node-induced confinement (typically associated with Pauli repulsion, though more general), orbital contraction and polarization – that each modulate kinetic energy during bond formation. Through analysis of a series of archetypal bonds, we show that an exquisite balance of energy-lowering delocalizing and localizing effects are dictated simply by atomic electron configurations, nodal structure and

electronegativities. The utility of this unified bonding theory is demonstrated by its application to explain observed trends in bond strengths throughout the periodic table, including main group and transition metal elements.

Introduction

Despite considerable efforts at the intersection of chemistry and physics over the past century,[1–11] disagreement about the origins of the chemical bond remain.[12–16] While there is general consensus that electron density increases in the internuclear region in a covalent bond—first defined by Langmuir as the sharing of electrons between atoms[3]—the causal connection between this density accumulation and the energy-lowering associated with covalency remains contested. Some, including Slater and Bader,[6,17] argue that this density accumulation is evidence that covalency results simply from the increase in electrostatic attraction arising from the introduction of a second nucleus; others, including Hellman and Ruedenberg,[7,8] instead invoke a purely quantum mechanical explanation by which the kinetic energy of the electron is lowered through the delocalization of this electron over an additional nucleus. A more pragmatic approach acknowledges that a bond is formed simply through constructive interference of quantum states,[4] without drawing further conclusions about the individual contributions of the kinetic and potential energy to lower the total energy.

Often invoked to provide both evidence and counter-evidence for the conflicting bonding theories of Slater and Hellmann, the virial theorem,[18]

$$2\langle T\rangle + \langle V\rangle + \sum_{\alpha}\sum_{\beta>\alpha} R_{\alpha\beta}\frac{\partial U}{\partial R_{\alpha\beta}} = 0 \tag{1}$$

connects the observable quantities $\langle T\rangle$ and $\langle V\rangle$ – the average kinetic and potential energy of the system, respectively – via the first derivative of the total Born-Oppenheimer energy ($U = T_{el} + V_{el} + V_{nn}$) with respect to internuclear distances $R_{\alpha\beta}$ (the so-called 'Feynman

force').[19,20] During bond formation, illustrated here for the simplest covalent bond between a hydrogen atom and a proton (Figure 1), initial lowering of the kinetic energy of the system occurs as the nuclei approach from large separation—in apparent agreement with Hellmann's explanation—however as the bond length decreases further towards its equilibrium distance, the kinetic energy increases to a value greater than that of separated atoms. The potential energy, conversely, initially increases relative to separated atoms, and becomes strongly binding towards the equilibrium bond length, in apparent agreement with Slater's interpretation. At equilibrium, the Feynman forces $^{\partial U}/_{\partial R_{\alpha\beta}}$ are zero, yielding the 'virial ratio' of $\langle T \rangle = -\frac{1}{2}\langle V \rangle$. The linear dependence of $\langle T \rangle$, $\langle V \rangle$, and these Feynman forces via eq. 1 has resulted in much disagreement in the search for a universal, causal framework to understand chemical bond formation. While access to $\langle T \rangle$ and $\langle V \rangle$ requires knowledge of only the total energy and the Feynman force, the reverse is also true, since the total energy is the sum of the kinetic and potential energies of the system, and the Feynman force can be obtained by taking its derivative with respect to $R_{\alpha\beta}$. To fully understand the origins of bond formation, we must therefore find the underlying mechanism that determines the direction of causality between each of these observable quantities. Consistent with energy decomposition analysis identifying driving forces for chemical bonding from constraints on quantum mechanical calculations,[21] we use the term 'causal' in the bottom-up sense.

In this paper, we attempt to uncover this causal connection by focusing on the controversy surrounding the cause of the increase in $\langle T \rangle$ as the bond approaches its equilibrium length. Ruedenberg and co-workers, using variational arguments and later a quasi-atomic orbital approach, showed that for H_2^+ and H_2, the contraction (*i.e.*, shrinking volume) of atomic orbitals is responsible for this increase in kinetic energy.[8,22–24] Such contraction is suggested to drive further electron delocalization (*i.e.*, additional energy lowering), such that while the *total* kinetic energy change becomes destabilizing, the *interatomic* portion of $\langle T \rangle$, associated with the sharing of the electron over both nuclei, continues to decrease as the bond length decreases. This result was corroborated by Levine & Head-Gordon[14] using

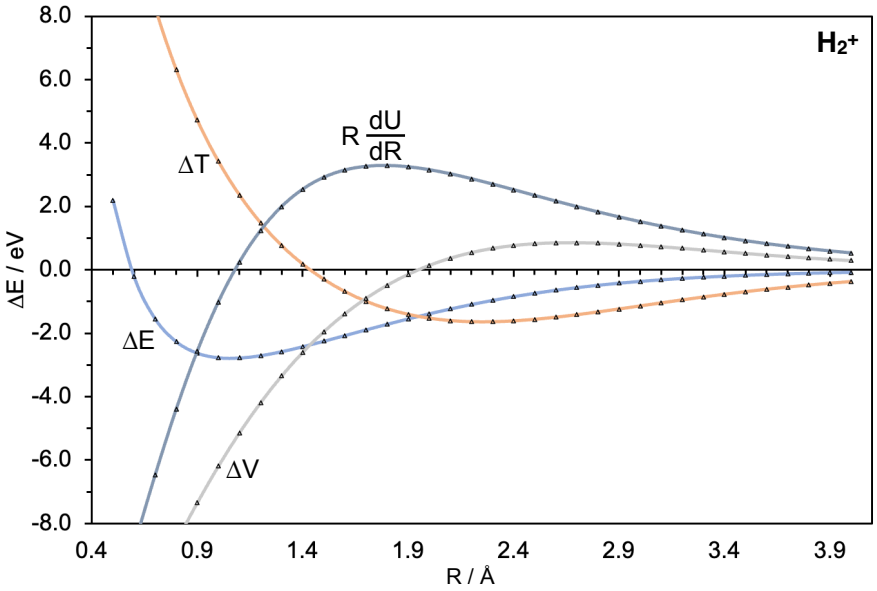

Figure 1: Decomposition of energy contributions to the H_2^+ bond, in eV, at the HF/cc-pVTZ level (*i.e.*, for the exact wavefunction in this basis).

the absolutely localized molecular orbital energy decomposition (ALMO-EDA) scheme for bonded interactions,[25–27] and later by Bacskay using a modified atomic orbital (MAO) approach.[16] The agreement between each of these methods for H_2^+ and H_2 offers strong evidence for the Hellmann description of covalent bonding in these systems: At short bond lengths orbital contraction offers a variational route to lower the total energy, enhancing interatomic electron delocalization while overall lowering the potential energy that ultimately restores the virial balance at equilibrium.

However, significant discrepancies appear to arise between these methods for bonds between heavy (non-hydrogen) atoms. Ruedenberg and co-workers reported that, as observed for H_2^+ and H_2, the interatomic kinetic energy contribution for first row homodiatomics (B_2, C_2, N_2, O_2 and F_2) is more stabilizing than that of the separated atoms at all bond lengths, and that contraction is again solely responsible for the intramolecular kinetic energy increase at equilibrium.[22,23] This result was later confirmed by Bacskay when examining both the systems studied by Ruedenberg and co-workers, as well as Li_2, CO, P_2, Cl_2, $CH_3{-}CH_3$, $CH_3{-}SiH_3$, $CH_3{-}OH$ and $CH_3CH_2{-}CH_2CH_3$.[16] In contrast, Levine and Head-Gordon, in

their study of $CH_3CH_2{-}CH_2CH_3$, $[CH_3CH_2{-}CH_2CH_3]^{\bullet+}$, $[Li_2]^{\bullet+}$, Li_2, F_2, and various second-row hydrides (LiH, $[BeH]^+$, HBe−H, BH, CH, HF), showed that orbital contraction effects only significantly lower the energy (and cause an increase in kinetic energy) for bonds involving hydrogen.[14] The kinetic energy increase associated with bond formation with heavy atoms was instead suggested to occur due to the overlap of core electrons. This result aligns with the valence bond interpretation in which non-bonded repulsions are suggested to play an important role in the spectrum of covalent → charge-shift → ionic bonding,[28] and leads to the conclusion that kinetic energy lowering cannot be the universal cause of covalency.

In this work, we construct an independent, easily-interpretable kinetic energy decomposition framework based on the configuration interaction wave function, separating total and kinetic energy changes arising due to orbital relaxation (*e.g.*, contraction) from those arising solely through electron delocalization. This framework is applied in the first instance to H_2^+ and H_2, before being extended to heavy atom homonuclear diatomics (Li_2, N_2, O_2, F_2), a polyatomic system ($H_3C{-}CH_3$), and heterodiatomics (LiH, HF). Further decomposition of the kinetic energy by symmetry offers a more detailed view of the importance of orbital contraction in multiply bonded molecules. Based on these results, we identify three mechanisms through which kinetic energy increases upon bond formation, constructing a single unified theory for bond formation while resolving the conflicting interpretations of Ruedenberg, Backskay, and Levine & Head-Gordon. These mechanisms are applied to interpret trends in main group and transition metal bonds, illustrating the utility of this unified bonding model to understand chemical trends and properties.

Methods and Methodological Considerations

To evaluate the importance of orbital contraction on bond formation, a complete active space (CAS)-based kinetic energy decomposition analysis (KEDA) was developed. The basic idea is to compare energy (and kinetic energy) changes that occur with a fully optimized CAS

wavefunction versus a wavefunction in which the active orbitals are constrained to span the space of isolated fragments (*i.e.*, prohibiting contraction,[26] as well as some other orbital relaxation effects[29] discussed below). This uncontracted CASCI wavefunction is constructed as follows: (1) Obtain a set of localized CASSCF (complete active space self-consistent field) molecular orbitals, $\{\phi\}$, for a given system in which the atoms/fragments are non-overlapping (this broken bond limit is chosen to be 10 Å here for neutral fragments and 1000 Å for charged fragments); (2) Use the active space spanned by these broken bond CASSCF orbitals as a basis for a subsequent CASCI (complete active space configuration interaction) calculation, in which the CI describes bonding in the absence of orbital relaxation. This approach decomposes total and kinetic energies into electron delocalization and orbital relaxation contributions while ensuring qualitatively correct dissociation of the molecule. The kinetic energy expectation value $\langle T \rangle$ is obtained analytically by taking Tr[$\mathbf{PT}$], where $\mathbf{P}$ is the one-particle density matrix and $\mathbf{T}$ is the kinetic energy matrix. Numerical evaluation of $\langle T \rangle$ for a range of systems suggests that non-Hellmann-Feynman contributions are insignificant for the systems studied here (see Supporting Information). We direct the reader to a complementary but distinct approach to study the importance of kinetic energy on bond strength by Gordon, Ruedenberg and co-workers, in which a bond order metric derived from scaled kinetic energy and density matrix elements in an adaptive minimal basis is employed to understand bonding in a variety of polyatomic systems.[30–39]

The CASCI $\{\phi\}$ are first obtained from the broken bond fragment-localized CASSCF $\{\phi\}$ by rigid translation to the target bond distance. As a result the initial CASCI $\{\phi\}$ are non-orthogonal. The CASCI energy (and other observables) are invariant to non-singular transformations of the active orbitals (such as orthogonalization), but not to mixings between active valence and inactive occupied orbitals. To avoid the need to necessarily correlate all core and valence electrons, we adopt a judicious orthogonalization procedure that separates the active and inactive occupied spaces. First we symmetrically orthogonalize all core (inactive) orbitals (eq 2a), followed by projection of the orthogonalized core out of the valence

(active) orbitals (eq 2b), and subsequent renormalization and symmetric orthogonalization of these projected valence orbitals:

$$\tilde{\mathbf{C}}_{\mathrm{c}} = \mathbf{C}_{\mathrm{c}}\mathbf{S}_{\mathrm{c}}^{-\frac{1}{2}} \tag{2a}$$

$$\mathbf{C}_{\mathrm{v,proj}} = (\mathbf{I} - \tilde{\mathbf{P}}_{\mathrm{c}}\mathbf{S}_{\mu\nu})\mathbf{C}_{\mathrm{v}} \tag{2b}$$

where $\mathbf{C}$ is the coefficient matrix, $\mathbf{S}$ is the overlap matrix, $\mathbf{P} = \mathbf{C}\mathbf{C}^{\mathbf{T}}$, subscripted c, v denote core and valence spaces, respectively, and μ, ν, denote atomic orbitals (see the Supporting Information for further details). For Li_2 this procedure with a full valence (2,2) active space was found to give qualitatively similar results to those obtained through symmetric orthogonalization of the full core/valence space (6,4) (see SI Figure S1). CAS natural orbital (NO) decomposition was subsequently carried out to obtain individual kinetic energy contributions of each NO by transformation of the $\mathbf{T}$ matrix into the NO basis, where NO symmetry was assigned by inspection.

With the use of broken-bond orbitals (BBO) for the CASCI and fully optimized orbitals for CASSCF, such that the two methods are identical at the limit ($E_{\mathrm{CASSCF}}(r_{\mathrm{BB}}) = E_{\mathrm{CASCI}}(r_{\mathrm{BB}})$), we can then express the energy (or kinetic energy) changes relative to the broken bond geometry (r_{BB}) as follows:

$$\Delta E(r) = E_{\mathrm{CASSCF}}(r) - E_{\mathrm{CASSCF}}(r_{\mathrm{BB}}) \tag{3}$$

$$= (E_{\mathrm{CASCI}}(r) - E_{\mathrm{CASSCF}}(r_{\mathrm{BB}})) + (E_{\mathrm{CASSCF}}(r) - E_{\mathrm{CASCI}}(r)) \tag{4}$$

$$\equiv \Delta E_{\mathrm{BBO}}(r) + \Delta E_{\mathrm{rlx}}(r) \tag{5}$$

We have therefore isolated all orbital relaxation effects in ΔE_{rlx}, while all energy lowering that is possible with the fixed broken bond orbitals is captured in ΔE_{BBO}. To be very clear, ΔE_{rlx} contains the effect of orbital contraction, which we want to focus on, as well as *all* other orbital relaxation effects which we shall refer to as orbital polarization (whose origin is not

just electrical, but includes the influence of electron delocalization, relaxation of Pauli repulsions, etc.). The contraction effect (shrinking orbital size) is associated with kinetic energy increase due to increasing electron confinement. Similarly, orbital polarization is equivalent to mixing the occupied orbital with an unoccupied orbital with higher orbital angular momentum, which will also increase the kinetic energy of the electron (this is necessarily true due to an increase in the number of nodes of the higher orbital). For clarity, we have deliberately avoided reusing any notation from the bonded ALMO-EDA,[14,25–27] as we would like our new analysis to be entirely independent from it. However, we would like to point out that while the spin coupling term in the bonded ALMO-EDA approach describes only the electron delocalization effect associated with covalency, our BBO wave function describes a mixture of both covalent and ionic (charge transfer) contributions, where this mixture is optimal for the given set of BBO orbitals. Of course both procedures add correctly to the total interaction energy (cf. Eq. 5). We also note that, while the left-right correlation captured by the CASSCF/CASCI formalism employed here results in a qualitatively correct description of bond dissociation, dynamic correlation is largely absent. However, such dynamic correlation effects will not change our qualitative conclusions, and indeed Ruedenberg's approach also relies on an active space formalism,[22–24] thus allowing direct comparisons to be made with our results.

All calculations were carried out using a locally modified version of the Q-Chem program package (version 6.0).[40] All calculations used the cc-pVTZ basis unless otherwise specified,[41] with active spaces that are specified case-by-case in the results. Such active spaces always correlate all electrons involved in the chemical bond, and provide a bonding and an antibonding orbital for each such electron pair. Some calculations use the full valence active space when this is larger than the pairing active space associated with the bonding electrons. All potential curves are reported relative to the 10 Å broken bond reference configuration (neutral fragments) or 1000 Å reference (charged fragments), as implied by the definitions in Eq. 5. Excited BBO orbitals for H_2^+ were generated from the 2s orbital from the first

valence excited state of the hydrogen atom at the HF/aug-cc-pVQZ level. The resulting contracted basis set parameters are reported in the Supporting Information. The structure of ethane was optimized at the ωB97M-V/cc-pVTZ level.[42]

Results

Bonding in H_2 and H_2^+

To test the validity of the KEDA approach developed here, the kinetic energy contributions to bond formation for H_2 and H_2^+ were compared with the results of Ruedenberg, Bacskay, and Levine & Head-Gordon.[8,14,16] For H_2 and H_2^+, ≈80% and ≈65% of the binding energy is recovered in the absence of orbital relaxation, respectively (Figure 2a and SI Figure S2). On their respective BBO surfaces, kinetic energy-lowering occurs as the H−H distance decreases from large separation, reaching minima at ≈1.2 and ≈1.5 r_e before rising slightly as the bond is further compressed. A similar initial kinetic energy decrease is seen on the fully relaxed surface, where minima are reached at a much earlier point (≈2 r_e for both H_2 and H_2^+). However, at shorter distances than twice r_e, the kinetic energy increase when the relaxation constraint is lifted is substantial, resulting in a positive kinetic energy contribution relative to separated atoms at the equilibrium bond length. These results support the theory that orbital relaxation—in this case contraction—causes the sharp increase in kinetic energy upon bond formation. We note, however, that even in the absence of orbital relaxation the kinetic energy does not decrease monotonically upon bond formation; we suggest that the small increase in kinetic energy at short bond lengths is the result of a decrease in bonding orbital volume. Finally, it is interesting to observe that orbital relaxation at long distances ($r \gtrapprox 2.5\ r_e$) *increases* the kinetic energy lowering. In this highly stretched bond regime, orbital contraction no longer occurs, and in fact very slight orbital *expansion* improves interfragment overlap to provide a small amount of additional binding (Figure 2b inlay) as shown by the red mesh outline (representing the relaxed orbital) surrounding the blue BBO orbital.

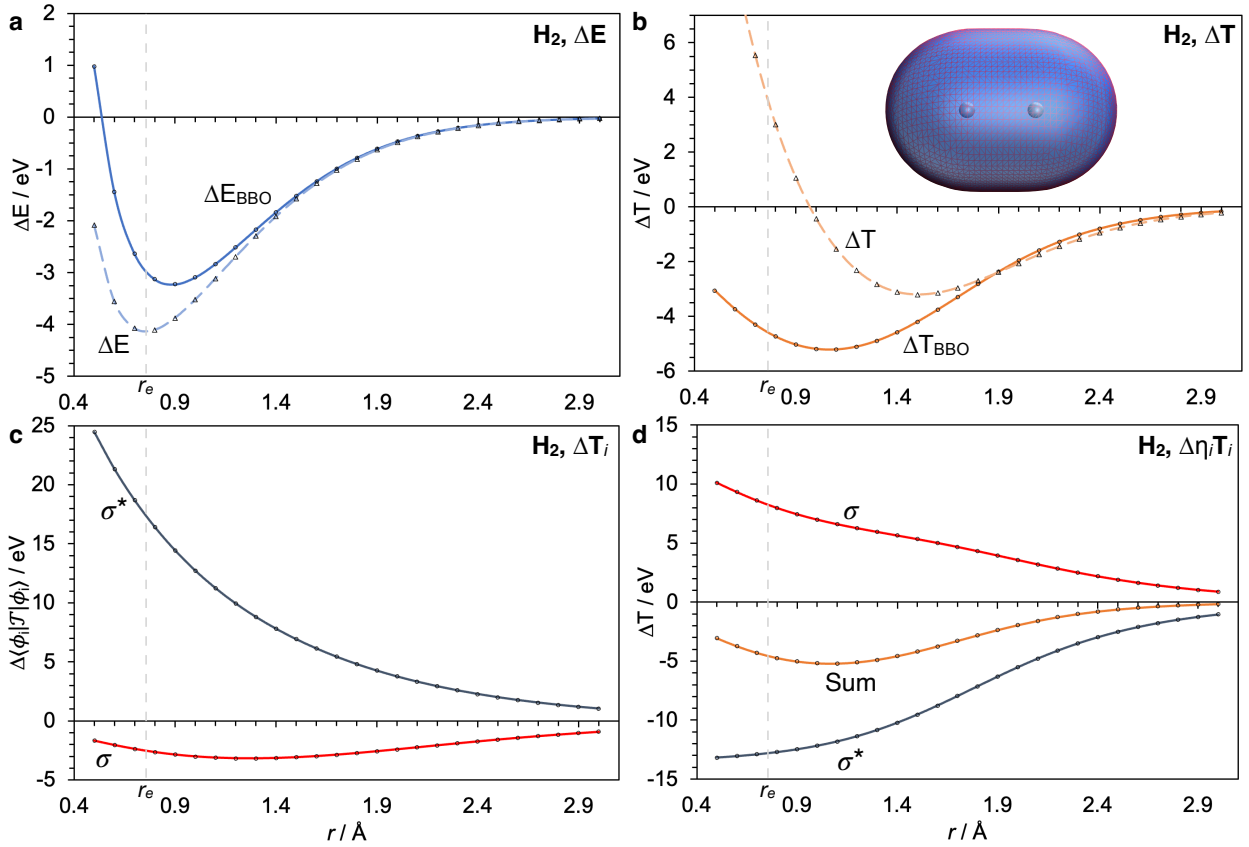

Figure 2: Total energy (**a**) and kinetic energy (**b**) decomposition of H_2 (CAS(2,2)/cc-pVTZ), and BBO natural orbital decomposition of $\langle T \rangle$ (**c**) and the contributions of these natural orbitals to ΔT via $\eta_i T_i$ (**d**). Vertical dashed lines denote $r_e = 0.755$ Å. Inlay: BBO (solid blue) and relaxed (red mesh) σ bonding natural orbitals for H_2 ($r = 2.4$ Å) containing 90% of the electron.

Decomposition of the H_2 bonding (σ) and anti-bonding (σ^*) broken bond natural orbital (NO) contributions to the kinetic energy change upon bond formation reveals that, as expected, the kinetic energy of the nodeless σ orbital is lower (more negative) than that of the isolated atomic orbitals at all distances (Figure 2c). The introduction of a node in the σ^* orbital causes its kinetic energy to increase steeply as the bond-length shortens. The kinetic energy contribution of each orbital to the *total* change in $\langle T \rangle$ is given by $\eta_i T_i$ (where η_i and T_i are the occupation number and kinetic energy, respectively, of the i^{th} NO). Interestingly, this contribution *increases* $\langle T \rangle$ at all distances for the σ orbital, and the σ^* orbital *decreases* $\langle T \rangle$ at all distances (Figure 2d). At large bond lengths, the σ and σ^* orbitals are equally populated, describing complete localization of the electron(s) onto each atom; depopulation

of the anti-bonding orbital captures the kinetic energy-lowering electron delocalization between atoms. Correspondingly, the increased occupation of the σ orbital coupled with its relatively flat distance dependence accounts for its KE-increasing contribution.

The role of the electron core

The importance of core orbitals on covalent bond formation was next examined using Li_2 as an isolobal analogy of H_2, but with the inclusion of an electron core. The BBO wave function recovers ≈70% of the total binding energy (Figure 3a), and as observed above for H_2, the kinetic energy decreases as the bond length decreases down to a minimum at ≈1.3 r_e. However, at odds with H_2, the BBO ΔT curve *rises above zero as the equilibrium bond length is reached* (Figure 3b), agreeing closely with the equivalent relaxed curve. Since *all* orbital relaxation effects are absent from the BBO wave function, such a rise in kinetic energy cannot be attributed to contraction. Given that the use of the BBO orbitals leads to the majority of the equilibrium binding energy, yet the kinetic energy increases versus fragments, this result directly contradicts the idea that kinetic energy lowering is a driver for chemical bonding.

Decomposition of the BBO kinetic energy by NO reveals qualitatively different behavior to H_2 (Figure 3c); while the kinetic energy of the σ NO initially decreases as the bond length decreases from large separation, it then increases above that of the separated atoms as the bond length decreases towards its equilibrium value. The kinetic energy of the σ^* NO follows an inverted trend, crossing the σ orbital kinetic energy at compressed bond lengths. The kinetic energy of the core is effectively constant at all bond lengths and can therefore be disregarded.

Projection of the valence σ NO along the bond axis as a function of bond length reveals a mechanism for kinetic energy increase that does not require orbital contraction or polarization (Figure 4). We see an increase in the magnitude of the bonding orbital near the nuclear cusp as the bond length decreases, which results from destructive overlap (Pauli exclusion)

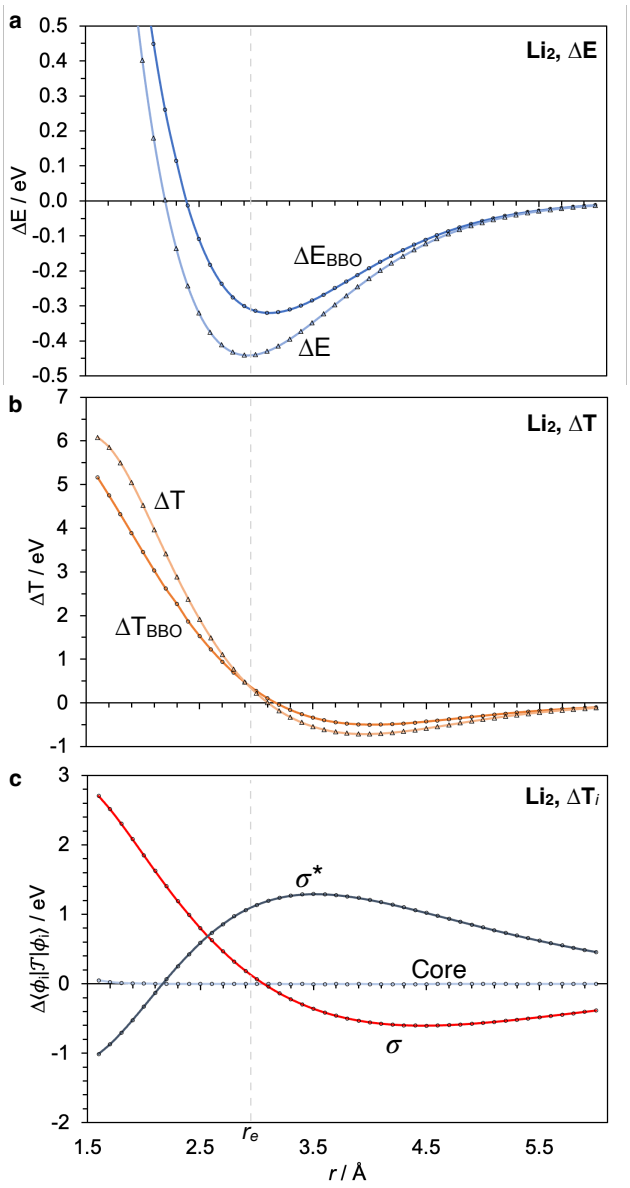

Figure 3: Total energy, kinetic energy and BBO natural orbital $\langle T \rangle$ decomposition of Li_2 (**a**–**c**, CAS(2,2)/cc-pVTZ). Vertical dashed lines denote $r_e = 2.931$ Å.

between the 2s valence orbital on the first atom and the 1s core on the second. We also see a decreasing distance between the radial nodes of the 2s orbitals on each atom, which progressively decreases the volume occupied by the delocalized electron (*i.e.*, the volume between the nodes) compared with the isolated atoms – effectively a node-induced electron confinement. Both of these consequences of Pauli exclusion contribute to the observed increase in kinetic energy towards the equilibrium bond length, and result in a weak covalent bond

(25.1 kcal mol^{-1} for Li_2, compared with 104.2 kcal mol^{-1} for H_2).[43] Indeed, similar analysis for H_2 reveals the expected constructive overlap associated with kinetic energy-lowering delocalization at all distances (see SI, Figure S3).

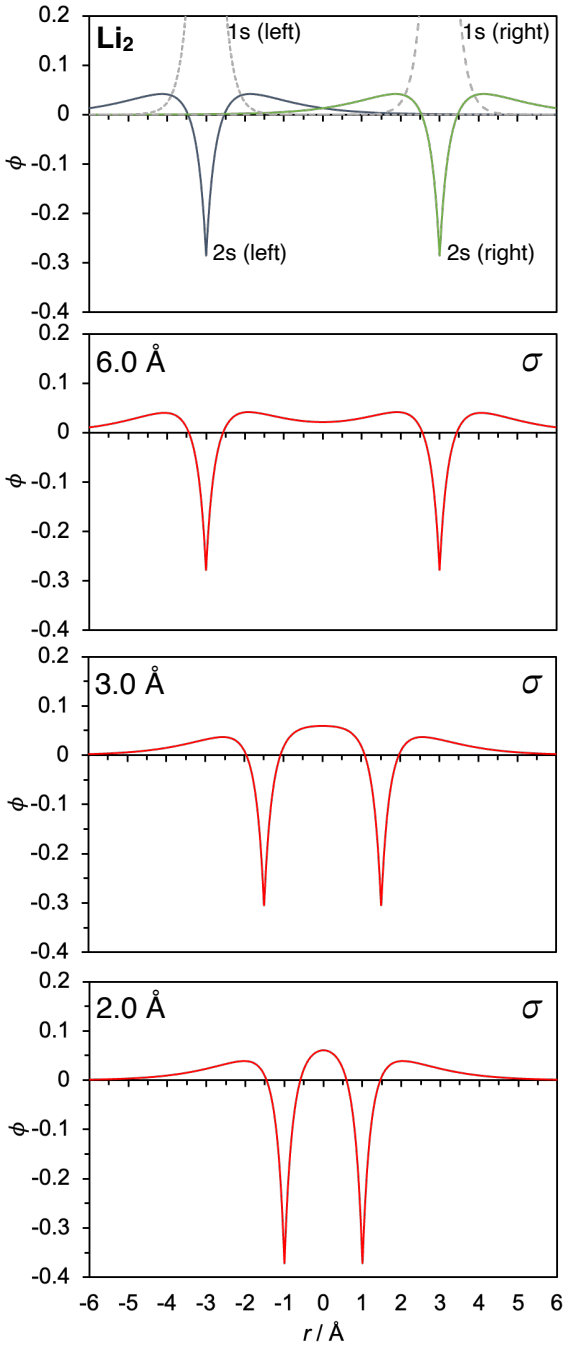

Figure 4: Projection of the z-component of the isolated atomic orbitals (top) and BBO σ natural orbital of Li_2 (CAS(2,2)/cc-pVTZ) as a function of bond length.

Node-induced confinement is typically a manifestation of Pauli repulsion in ground state

molecules. After all, Pauli exclusion creates nodes when occupied levels from different fragments with like spins overlap and are reorthogonalized to obey the Pauli principle. However, node-induced confinement can also sometimes exist independently as a consequence of quantization. For example, the bond formed from a single electron in an excited state of H_2^+ formed from a pair of 2s orbitals has nodal structure but lacks an electron core; such a bond may then suffer from node-induced confinement but is strictly free of Pauli repulsions (Figure 5a). Compared with the H_2^+ bond formed from H 1s BBOs (*i.e.*, ground state H_2^+), with 2s BBOs delocalization is substantially diminished, reaching a minimum in the kinetic energy only $\approx 40\%$ as low (Figure 5b). Node-induced confinement certainly arises from Pauli repulsion, but as this excited H_2^+ example illustrates, it can also arise independently due to radial nodes – whose importance in the context of bonding has previously been emphasized.[44,45] Henceforth we shall employ the term 'node-induced confinement', as a generalization of Pauli repulsion.

To further explore these node-induced confinement mechanisms, we next investigated the effect of localization on the strength of ionized covalent bonds, which dissociate to charged, rather than neutral, fragments. Interestingly, while ionization of H_2 weakens the H−H bond,[43] the opposite is true of Li_2 – the Li−Li bond in Li_2^+ has a *higher* dissociation energy than the neutral molecule.[43,46,47] The qualitative difference between the bonding in H_2^+ and Li_2^+ was previously noted by Müller and Jungen,[48] who suggested that 2s/2pσ polarization in Li_2^+—absent in H_2^+—is responsible for the contrasting kinetic energy profiles that accompany bond formation.

The BBO surface for Li_2^+ (see SI, Figure S4) reveals no binding, such that orbital relaxation is entirely responsible for the Li−Li bond. We suggest that while node-induced confinement negates covalent stabilization on the BBO surface of Li_2^+, induced electrostatic stabilization that is captured through orbital polarization (*e.g.*, an ion-induced dipole interaction) stabilizes Li_2^+. This induced electrostatic effect in Li_2^+ is larger than the covalent stabilization in Li_2 due to the nodal structure of the 2s orbitals, such that the Li−Li bond

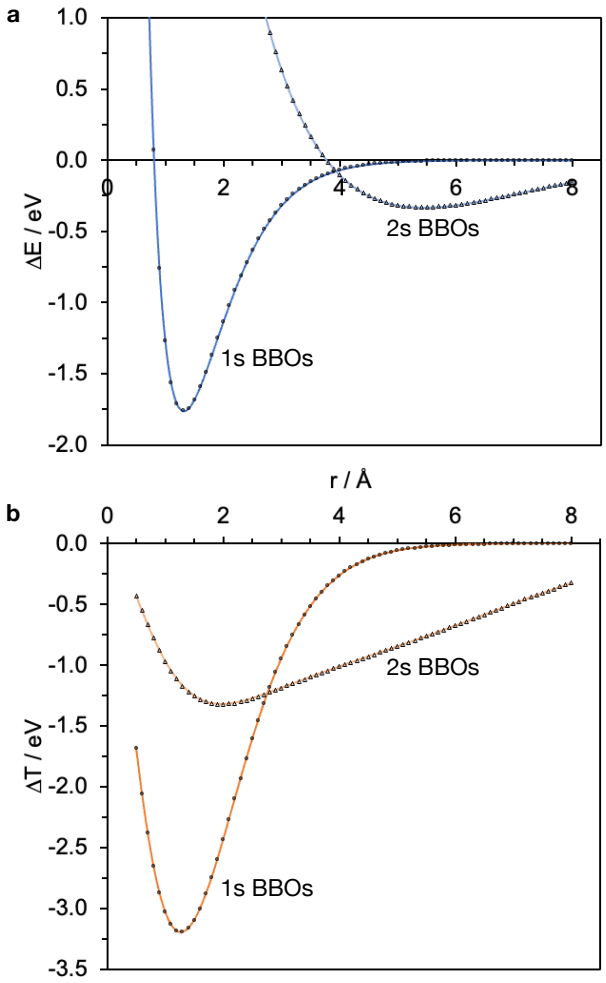

Figure 5: Total energy (a) and kinetic energy (b) of H_2^+ (HF/BBO), where '1s' denotes BBOs formed from optimal H 1s orbitals, and '2s' denotes BBOs formed from optimal H 2s orbitals of the first valence excited state of H, each generated from an aug-cc-pVQZ basis.

becomes *stronger* upon ionization. Crucially, the far stronger covalency in H_2 than Li_2—due to the absence of nodal structure in the 1s valence orbitals of H—dominates any bond-strengthening induced electrostatic stabilization in H_2^+, and the H−H bond weakens upon ionization as a result.

We next considered whether the localizing effect of node-induced confinement plays a role in the formation of the C−C bond of ethane. As methyl radical fragments approach, once again kinetic energy decreases as the bond begins to form due to electron delocalization (Figure 6a and 6b), before rising steeply in the absence of orbital relaxation as the bond

length approaches its equilibrium value. However, unlike Li_2 or H_2, orbital relaxation in $CH_3{-}CH_3$ *decreases* the amount of kinetic energy lowering at all bond lengths relative to the use of constrained BBO orbitals. This is a curious result; if kinetic energy lowering is responsible for bond formation, then at long bond lengths (where contraction is unequivocally negligible), the kinetic energy decrease should be *maximized* upon variational orbital relaxation. Clearly orbital relaxation is dominated by effects other than contraction, and we suggest that orbital polarization, which in a valence bond picture will increase the stability of ionic ($CH_3^+ \cdots CH_3^-$ and $CH_3^- \cdots CH_3^+$) configurations, sacrifices covalent kinetic energy lowering to minimize the total energy. Both the equilibrium result and the stretched bond results again call into question the universality of the kinetic energy-lowering mechanism for bond formation.

To further explore the role of covalent–ionic resonances on changes in kinetic energy during bond formation, we examined the charge-shift bond of F_2. This bond is characterized by significant resonance between covalent and ionic structures,[49] which is suggested to relieve kinetic energy-increasing interatomic electronic repulsion that arises due to the 'lone-pair bond weakening effect',[28,50] thus restoring the virial balance.

Using our KEDA approach, initial kinetic energy lowering on the BBO surface is followed by an increase in ΔT above zero as the bond approaches its equilibrium length (Figure 6c and 6d), in a manner similar to that of the covalent Li_2 and $CH_3{-}CH_3$ bonds. This result suggests that contraction cannot be the primary cause of the kinetic energy increase accompanying bond formation. Repulsion is greater for F_2 than both Li_2 and CH_3–CH_3 due to the increased number of core-valence and valence-valence non-bonding interactions, but the general kinetic energy-raising mechanism is the same. The importance of ionic resonance structures in the F_2 bond is again manifested through an *increase* in the kinetic energy upon orbital relaxation relative to the BBO wave function, as was seen for $CH_3{-}CH_3$.

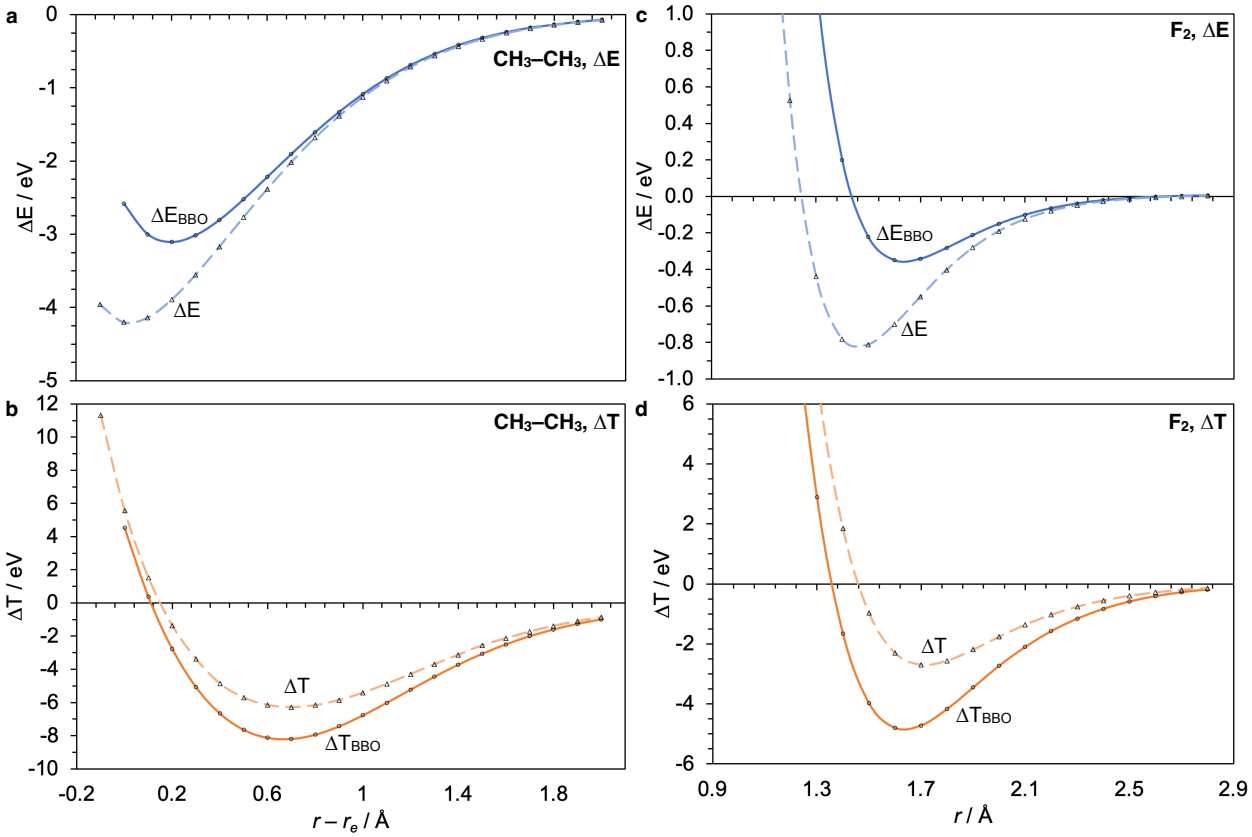

Figure 6: Total and kinetic energy decomposition of $CH_3{-}CH_3$ (**a**–**b**, CAS(2,2)/cc-pVTZ), and F_2 (**c**–**d**, CAS(14,8)/cc-pVTZ).

Multiple bonds

Having identified three causes for the increase in kinetic energy that accompanies bond formation (node-induced confinement, orbital contraction and polarization), the interplay of each of these mechanisms was studied in the context of multiple bond formation. The BBO wave function for N_2 (Figure 7a), which recovers ≈45% of the total binding energy, shows a substantial drop in kinetic energy as the bond length decreases from large separation (Figure 7b), reaching a minimum value of ≈–28 eV at ≈1.2 r_e. After this point, $\langle T \rangle$ begins to increase but does not exceed the value of the isolated atoms until the bond is compressed to distances smaller than its equilibrium length. Orbital relaxation causes a marked increase in the kinetic energy; after reaching a shallower minimum on the relaxed ΔT surface at ≈1.4 r_e ($\Delta T \approx$ –16 eV), ΔT rises sharply to become positive prior to reaching the equilibrium

bond length.

Decomposition of the N_2 bond into σ and π components reveals starkly different behavior of each system (Figure 7c). On the one hand, the π components of the BBO and relaxed kinetic energy surfaces exhibit a qualitative resemblance to the ΔT curves of H_2 and H_2^+, suggesting significant contraction effects. On the other hand, the σ framework is simultaneously behaving in a manner more similar to the covalent bonds in Li_2 and F_2. In fact, as observed for F_2, orbital relaxation once again *increases* ΔT relative to the BBO wave function, illustrating the importance of charge transfer on the nature of the σ bond of N_2.

These results can be explained by considering the nodal structure and symmetry of the constituent atomic orbitals in the N_2 bond: while overlap of sp hybrids—inheriting a radial node from the 2s orbital—along the bond axis causes an increase in kinetic energy in the absence of contraction, the π orbitals formed through side-on overlap of pairs of $2p_x$ and $2p_y$ orbitals do not suffer from the same node-induced electron localization due to their orthogonality with the 1s core and sp hybrids on the opposing atom, and may instead contract to increase the kinetic energy. Due to the zero amplitude of p orbitals at the nucleus, this contraction incurs less of an energetic penalty from Pauli repulsion with its own core. These separable σ and π effects balance such that the total energy is minimized. Similar conclusions were reached by Hirshfeld and Rzotkiewicz based on promolecular electrostatic arguments.[51]

To investigate the generality of this description of multiple bonding, we next considered the double bond of O_2 in its ground (triplet) state, where ≈40% of the total bond energy is recovered by the BBO wave function (Figure 7d). A qualitatively similar trend to N_2 is observed for the variation of the kinetic energy with decreasing bond length (Figure 7e), albeit with a less pronounced kinetic energy decrease at longer bond lengths, and a sharper rise in ΔT near the equilibrium bond length. NO decomposition of ΔT_{BBO} into σ and π components reveals that while the behavior of the σ system is similar to N_2 (Figure 7f), the kinetic energy of the π framework now also increases as the bond approaches its equilibrium

length. Compared with N_2, the additional pair of same-spin electrons in the π system of O_2 results in an antibonding interaction (*i.e.*, a new node arises due to Pauli exclusion) that progressively increases the kinetic energy of the π system as the orbital overlap increases. The O=O bond is therefore substantially weaker than the N≡N bond (118.9 vs 225.8 kcal mol^{-1}, respectively).[43]

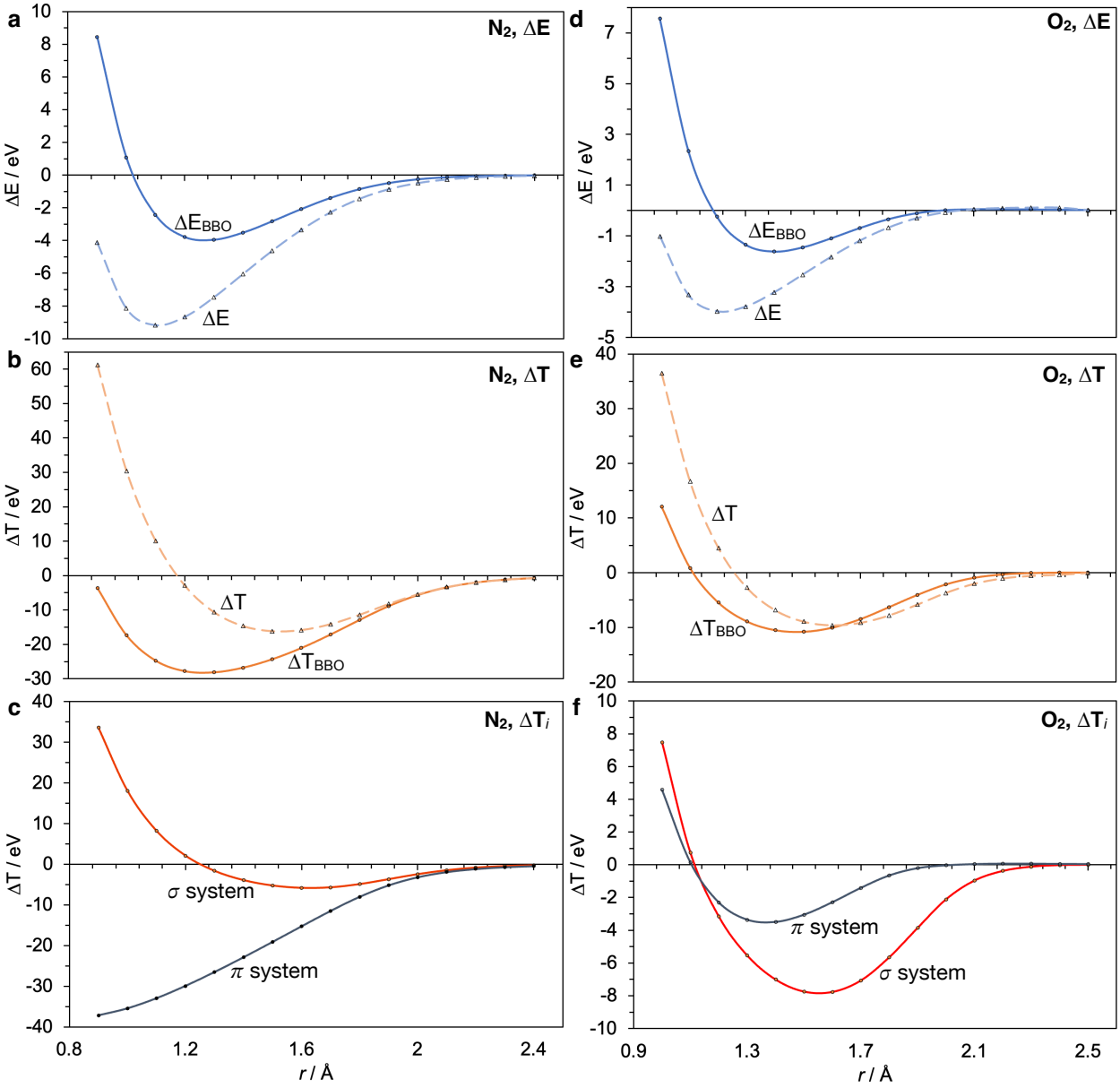

Figure 7: Total energy, kinetic energy, and natural orbital decomposition of N_2 (**a**–**c**, CAS(10,8)/cc-pVTZ) and O_2 (**d**–**f**, CAS(12,8)/cc-pVTZ).

Orbital contraction in heterodiatomics

We next considered the role of orbital contraction on the formation of bonds with a permanent dipole. To complete the isolobal comparison with H_2 and Li_2, we investigated the variation in kinetic energy accompanying formation of the LiH bond. The BBO wave function captures ≈70% of the total binding energy (Figure 8a), and the general trend in ΔT_{BBO} follows that of Li_2 (Figure 8b). As for Li_2, we suggest that as the bond length approaches its equilibrium value, node-induced confinement causes the kinetic energy to increase, in this case due to both H 1s / Li 1s and H 1s / Li 2s overlap.

At odds with all non-polar systems studied so far, orbital relaxation causes a *decrease* in kinetic energy at all bond lengths. A qualitative comparison of the BBO and relaxed σ bonding natural orbitals (Figure 8b, inlay) reveals that contraction occurs primarily in the vicinity of the lithium atom, and to a much smaller degree near the hydrogen atom. This contraction is accompanied by a substantial increase in the ionicity of the bond, illustrated by the increase in the negative charge on hydrogen during bond formation (Figure 8c). Orbital relaxation therefore appears to stabilize ionic configurations—as above for $CH_3{-}CH_3$ and F_2—but is not accompanied by the same increase in kinetic energy. The kinetic energy is not only the result of the shape and size of the orbital, but also its *occupation*; by reducing the electron population on the lithium atom, reduced on-site Pauli repulsion between the valence and core electrons means that contraction can now (slightly) lower the total energy *without increasing the kinetic energy.*

The importance of contraction in heterodiatomics was further explored by considering HF, a diatomic with an opposing dipole to LiH. Approximately 55% of the total bond energy is recovered by the BBO wave function (Figure 8d), and the kinetic energy once again increases in the absence of orbital relaxation. The importance of orbital relaxation on ΔT is significantly more pronounced than in LiH (Figure 8e), despite the similar ionic character of the two bonds according to their hydrogen partial charge magnitudes (but with opposite sign, Figure 8c and 8f). To account for the far greater ΔT lowering in HF than

LiH we propose the following: Asymmetric orbital contraction increases the delocalization of electron density from the less electronegative atom to the more electronegative atom. In the case of LiH, where χ(Li) = 0.98 and χ(H) = 2.20,[52] this contraction occurs primarily on the lithium atom (Figure 8b, inlay), but due to its filled 1s core, such a contraction is penalized by intra-atomic core-valence repulsion so has only a small stabilizing effect during bond formation. However, for HF, where χ(F) = 3.98,[52] contraction occurs primarily in the vicinity of the less electronegative hydrogen atom (Figure 8e, inlay), with negligible contraction in the vicinity of the fluorine atom. The lack of an electron core in the hydrogen atom means that this contraction occurs without inhibition, efficiently transferring electron density towards the fluorine atom to lower both the total energy and the kinetic energy of the system. These results may explain the greater bond strength of HF than LiH (136.2 vs 56.9 kcal mol^{-1}, respectively).

Notably, the effect of orbital relaxation on ΔT of polar bonds at equilibrium opposes that of *all* non-polar bonds studied here. Charge density must be symmetrically distributed in symmetrical systems; orbital contraction cannot be accompanied by a decrease in orbital occupation and therefore must increase ΔT at equilibrium.

Discussion

A unified theory for chemical bond formation

With each of these results in mind, we present a unified picture of the origin of bond formation. Chemical bonds at equilibrium geometry are characterized by a lowering of total energy and an increase in kinetic energy, as prescribed by the virial theorem.[6,18] Electron delocalization associated with constructive interference of atomic wave functions,[4] which depends on the overlap of valence orbitals, lowers the total energy of the system. For bonds formed from charged fragments, long-range interactions, for instance permanent and induced electrostatic interactions, may also lower the energy of the system.

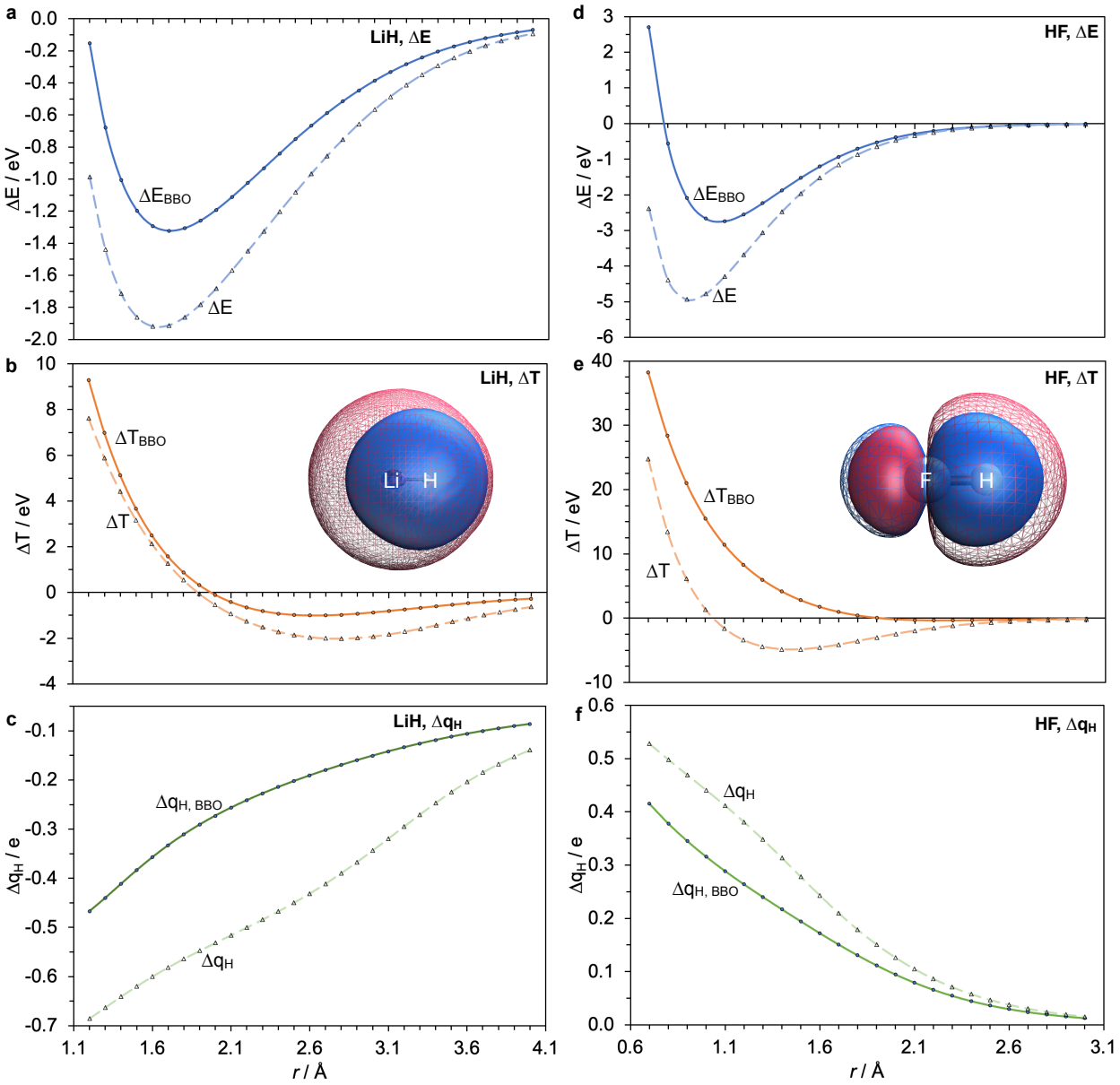

Figure 8: Total energy and kinetic energy decomposition, and partial charge analysis of LiH (**a**–**c**, CAS(2,2)/cc-pVTZ) and HF (**d**–**f**, CAS(10,6)/cc-pVTZ). Inlays: BBO (mesh) and relaxed (solid) σ bonding natural orbitals for LiH and HF containing 90% of the electron. Partial charges were calculated using the intrinsic atomic orbital method.[53]

As atoms approach, however, their orbitals start to overlap more significantly, and the following three processes may also occur (each to varying degrees):

1. *Node-induced confinement*: Electron delocalization (constructive interference) serves to stabilize a system, while the introduction of new nodes is destabilizing. The classic

origin of additional nodes is Pauli repulsion arising from overlap of filled orbitals. In the bonding context, with cores too compact to overlap significantly, Pauli repulsion arises from overlap of a (half-occupied) valence orbital with a filled orbital on a different atom to increase nodal structure in the resulting occupied orbital. Node-induced confinement thus typically arises from Pauli repulsion, though it can also arise due to overlap between a valence orbital with a node and an unoccupied or partially occupied valence orbital on a different atom, which also increases the nodal structure of the resulting bonding orbital. As the bond length decreases, this nodal structure becomes more pronounced, resulting in an increasingly localized electron and an increase in both the kinetic energy and total energy of the system.

2. *Orbital contraction*: Valence orbital contraction (shrinkage) effectively squeezes the electron to maximize on-atom kinetic energy, encouraging energy-lowering delocalization from one atom to another. This contraction is penalized by Pauli repulsion with the electron core, hence the importance of contraction in the core-less H_2 and H_2^+, and the lack of contraction in heavier non-polar bonds.

3. *Orbital polarization*: Valence orbitals may also change shape to stabilize ionic configurations that mix with the covalent bond to lower the energy. Such shape changes (polarizations), which are equivalent to mixing higher angular momentum orbitals into the wave function, will increase the kinetic energy of the resultant orbital, which is offset by a decrease in the potential energy to lower the total energy of the molecule.

For a non-polar bond (*e.g.*, H_2, $CH_3{-}CH_3$, F_2), any orbital relaxation must occur symmetrically, and will always increase the kinetic energy of the molecule. This restriction does not apply to polar bonds, which avoid this kinetic energy increase by redistributing electrons away from contracting orbitals.

At the equilibrium bond length, delocalizing and localizing effects balance such that the potential energy of the molecule is exactly –2 times the kinetic energy. How this virial

balance is reached depends on the nature of the atoms that comprise the bond, and is the subject of the following discussion.

Periodic trends in bond strengths

Both electronegativity differences and Pauli repulsion have previously been proposed as important factors that determine bond dissociation energies (BDEs).[10,54–56] To demonstrate the value of the mechanisms uncovered from our KEDA, we offer a unified picture that explains observable trends in experimental BDEs across the periodic table [BDEs (kcal mol^{-1}) in parentheses,[43] electronegativity difference of A−B[52] defined as $\Delta\chi \equiv \chi_B - \chi_A$]:

1. **H**–**H** (104.2) vs **Li**−**Li** (25.1) vs **Li**−**H** (56.9):

   The absence of core electrons in H−H enables energy lowering through orbital contraction. Contraction is prohibited in Li−Li due to the electron cores, and node-induced localization due to the higher principal quantum number of the valence orbitals causes severe bond weakening. While this same node-induced localization effect results in a weaker Li−H bond than H−H, charge transfer from Li to H ($\Delta\chi = 1.22$) enables modest contraction on Li to stabilize the bond.

2. **Li**−**H** (56.9) vs **H**−**F** (136.2) vs **Li**−**F** (138.0):

   Orbital contraction on the less electronegative atom occurs with charge transfer away from this atom to increase the bond strength. In Li−H this charge transfer occurs from Li to H ($\Delta\chi = 1.22$), however contraction is inhibited due to its electron core. In H−F, charge transfer *away from* H ($\Delta\chi = 1.78$) results in contraction on H, which substantially strengthens the bond due to the absence of a core. For Li−F, we predict that the considerable increase in the electronegativity difference ($\Delta\chi = 3.00$) depletes electron density on Li to the extent that contraction on Li now substantially increases the bond strength.

3. **H−F** (136.2) vs **H−Cl** (103.1) vs **H−Br** (87.5) vs **H−I** (71.3):

   Bond weakening down Group XVII occurs due to increasing node-induced localization as the number of nodes in the valence bonding orbital increases (resulting from a combination of overlap of valence orbitals with nodes, and increasing numbers of electrons in the core). Charge transfer from H to the halogen also decreases down the group due to the decrease in χ down Group XVII (3.98, 3.16, 2.96 and 2.66 for F, Cl, Br and I, respectively), decreasing the extent of energy-lowering orbital contraction on the H atom. These two effects act in the same direction to weaken the bond down the group.

4. **F−F** (37.9) vs **Cl−Cl** (58.0) vs **Br−Br** (46.3) vs **I−I** (36.4):

   As for the previous comparison, the gross trend of bond weakening occurs due to the increasing number of nodes in the valence σ bonding orbital. This trend is tempered by decreasing node-induced localization in the (fully occupied) π system as the X−X distance increases (which itself occurs due to optimization of σ overlap to balance delocalization and node-induced localization in the σ system), alongside a contribution from increasing polarizability that stabilizes ionic configurations. The result of these opposing effects is a non-linear BDE trend, with similarly weak F−F and I−I bonds. Contraction is negligible in these molecules due to the presence of the electron core and the lack of a permanent dipole.

5. $\mathbf{N_2}$ (225.8) vs $\mathbf{P_2}$ (116.9) vs $\mathbf{As_2}$ (91.3) vs $\mathbf{Sb_2}$ (71.8) vs $\mathbf{Bi_2}$ (48.9):

   As discussed above (Figure 7), the strength of the π bond in N_2 can be attributed to the lack of radial nodes in the 2p orbitals of N, thereby avoiding node-induced confinement effects in the resulting π system. Descending Group XV, however, increasing numbers of radial nodes contribute to the node-induced localization effect that weakens the π bonds of these diatomics.

6. **X−X vs** $[\mathbf{X{-}X}]^+$ (Figure 9):

Whether ionization of a molecule increases or decreases the BDE depends on the bonding mechanism, with a clear cutoff between two categories of bonds. In H−H, N≡N, and heterodiatomics, ionization weakens the bond, since the removal of an electron reduces the extent of *stabilizing* delocalization and contraction effects. This reduction outweighs any induced electrostatic effects that stabilize the ionized molecule. In contrast, bonds that suffer from node-induced localization benefit from ionization because the loss of modest delocalization stabilization is fully compensated by a combination of reduced Pauli repulsions and the emergence of induced electrostatic stabilization in the ionized molecule, resulting in net bond strengthening.

7. **H−Cr(Cp)(CO)$_3$** (61.5) vs **H−Mo(Cp)(CO)$_3$** (69.3) vs **H−W(Cp)(CO)$_3$** (72.4): These bonding mechanisms can also be applied to bonds involving transition metals. In the case of Group VI M−H bonds, increasing the numbers of nodes in the metal valence orbital will have a bond-weakening effect. However, the electronegativity of the metal also increases down the group (χ = 1.66, 2.16 and 2.36 for Cr, Mo and W, respectively), progressively increasing charge transfer away from H in the metal complex and strengthening the bond through contraction. This latter effect dominates the trend, leading to an increase in the M−H BDE down the group.

These explanations demonstrate the utility of the bonding mechanisms identified here, allowing us to explain experimental trends using a small number of competing effects.

Conclusions

Through the development of a simple method that separates total and kinetic energy changes into electron delocalization and orbital contraction contributions, we have developed a unified theory to explain the origins of chemical bonding. This unification resolves apparent conflicts between previous theories, which arise due to differences in interpretation, rather than methodological errors. We propose a set of mechanisms that accompany bond forma-

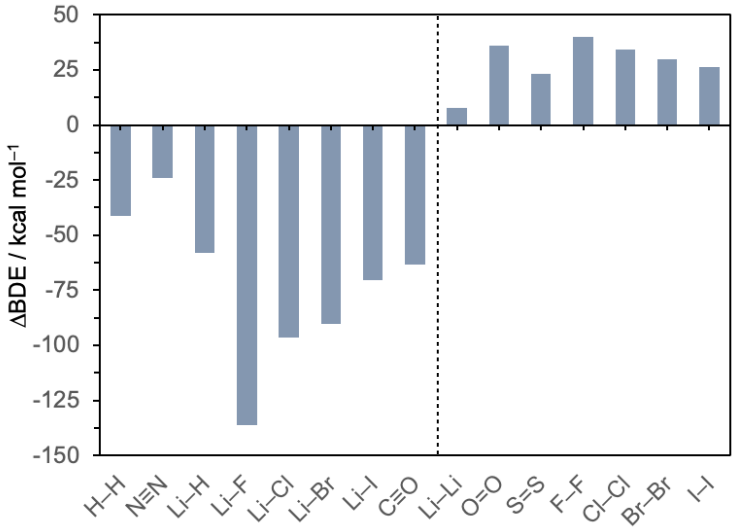

Figure 9: Difference in neutral and ionized bond dissociation energies [ΔBDE = $\mathrm{BDE}_{[\mathrm{X-X}]^+} - \mathrm{BDE}_{\mathrm{X-X}}$] in kcal mol^{-1}

tion, illustrating the exquisite balance of each to minimize the total energy of the system. The kinetic energy changes that accompany bonding are a result of the attenuation of electron delocalization by the introduction of nodes through valence-valence and core-valence interactions, and the change in size and shape of the atomic orbitals to balance covalent and ionic resonance structures such that the total energy is minimized. We apply these mechanisms to analyze a selection of main group and transition metal systems, showing that drastic changes in bonding accompany what appear to be only small differences in arrangements of electrons and nuclei. These differences can be understood almost entirely in terms of electronegativities and orbital nodal structure, and it is the unique combination of these factors for each element that gives rise to the rich chemistry of the periodic table.

Supporting Information

Additional computational details, methods, and discussion; full breakdown of total/kinetic/potential energies for all systems, and results of numerical tests (Figures S1–S6) (PDF).

Cartesian coordinates of optimized molecular geometries, and raw energies used to generate plots (Zip).

Conflicts of Interest

MHG is a part-owner of Q-Chem Inc, whose software was used for all developments and calculations reported here.

Acknowledgements

This work was supported by the U.S. Department of Energy, Office of Science, Office of Advanced Scientific Computing, and Office of Basic Energy Sciences, via the Scientific Discovery through Advanced Computing (SciDAC) program, with additional support from the U.S. National Science Foundation through Grant No. CHE-1955643 and CHE-2313791. We thank Devin Hernandez and Stephen Quiton for helpful discussions.

Author contact information

Alistair J. Sterling: Pitzer Center for Theoretical Chemistry, Department of Chemistry, University of California, Berkeley, California, 94720, United States

Daniel S. Levine: Pitzer Center for Theoretical Chemistry, Department of Chemistry, University of California, Berkeley, California, 94720, United States

Abdulrahman Aldossary: Department of Chemistry, University of Toronto, Toronto, Ontario, M5S 3H6, Canada

Martin Head-Gordon: Pitzer Center for Theoretical Chemistry, Department of Chemistry, University of California, Berkeley, California, 94720, United States

References

(1) Lewis, G. N. The Atom and the Molecule. *J. Am. Chem. Soc.* **1916**, *38*, 762–785.

(2) Kossel, W. Über Molekülbildung als Frage des Atombaus. *Ann. Physik* **1916**, *354*, 229–362.

(3) Langmuir, I. The arrangement of electrons in atoms and molecules. *J. Am. Chem. Soc.* **1919**, *187*, 359–362.

(4) Heitler, W.; London, F. Wechselwirkung neutraler Atome und homöopolare Bindung nach der Quantenmechanik. *Z. Phys.* **1927**, *44*, 455–472.

(5) Pauling, L. The Nature of the Chemical Bond. Application of the Results Obtained from the Quantum Mechanics and from a Theory of Paramagnetic Susceptibility to the Structure of Molecules. *J. Am. Chem. Soc.* **1931**, *53*, 1367–1400.

(6) Slater, J. C. The virial and molecular structure. *J. Chem. Phys.* **1933**, *1*, 687–691.

(7) Hellmann, H. Zur Rolle der kinetischen Elektronenenergie für die zwischenatomaren Kräfte. *Z. Phys.* **1933**, *85*, 180–190.

(8) Ruedenberg, K. The Physical Nature of the Chemical Bond. *Rev. Mod. Phys.* **1962**, *34*, 326–376.

(9) Feynman, R.P.; Leighton, R.B.; Sands, M. *The Feynman Lectures on Physics, Volume III: Quantum Mechanics*; Addison-Wesley Publishing Company, Inc.: Reading, MA, USA, 1965; pp 10–1.

(10) Kutzelnigg, W. The Physical Mechanism of the Chemical Bond. *Angew. Chem. Int. Ed. Engl.* **1973**, *12*, 546–562.

(11) For a recent review, see: Zhao, L.; Pan, S.; Holzmann, N.; Schwerdtfeger, P.; Frenking, G. Chemical bonding and bonding models of main-group compounds. *Chem. Rev.* **2019**, *119*, 8781–8845.

(12) Rioux, F. Kinetic Energy and the Covalent Bond in H_2^+. *Chem. Educator* **1997**, *2*, S1430–4171(97)06153–2.

(13) Nordholm, S.; Bacskay, G. B. The basics of covalent bonding in terms of energy and dynamics. *Molecules* **2020**, *25*, 2667.

(14) Levine, D. S.; Head-Gordon, M. Clarifying the quantum mechanical origin of the covalent chemical bond. *Nat. Commun.* **2020**, *11*, 4893.

(15) Martín Pendás, Á.; Francisco, E. The role of references and the elusive nature of the chemical bond. *Nat. Commun.* **2022**, *13*, 3327.

(16) Bacskay, G. B. Orbital contraction and covalent bonding. *J. Chem. Phys.* **2022**, *156*, 204122.

(17) Bader, R. F. Worlds apart in chemistry: A personal tribute to J. C. Slater. *J. Phys. Chem. A* **2011**, *115*, 12667–12676.

(18) Hurley, A. C. Virial Theorem for Polyatomic Molecules. *J. Chem. Phys.* **1962**, *37*, 449–450.

(19) Feynman, R. P. Forces in molecules. *Phys. Rev.* **1939**, *56*, 340–343.

(20) Gupta, V. *Principles and Applications of Quantum Chemistry*; Elsevier, 2016; pp 339–357.

(21) Mao, Y.; Loipersberger, M.; Horn, P. R.; Das, A.; Demerdash, O.; Levine, D. S.; Prasad Veccham, S.; Head-Gordon, T.; Head-Gordon, M. From intermolecular interaction energies and observable shifts to component contributions and back again: A

tale of variational energy decomposition analysis. *Ann. Rev. Phys. Chem.* **2021**, *72*, 641–666.

(22) Schmidt, M. W.; Ivanic, J.; Ruedenberg, K. Covalent bonds are created by the drive of electron waves to lower their kinetic energy through expansion. *J. Chem. Phys.* **2014**, *140*, 204104.

(23) Schmidt, M. W.; Ivanic, J.; Ruedenberg, K. *The Physical Origin of Covalent Binding*; Chapter 1, pp 1–67, In the book: The Chemical Bond. Fundamental Aspects of Chemical Bonding, Edited by Frenking, G., Shaik, S., Wiley-VCH, Weinheim, Germany, 2014.

(24) Ruedenberg, K. Atoms and bonds in molecules as synergisms of interactions between electrons and nuclei. *J. Chem. Phys.* **2022**, *157*, 210901.

(25) Levine, D. S.; Horn, P. R.; Mao, Y.; Head-Gordon, M. Variational energy decomposition analysis of chemical bonding. 1. Spin-pure analysis of single bonds. *J. Chem. Theory Comput.* **2016**, *12*, 4812–4820.

(26) Levine, D. S.; Head-Gordon, M. Quantifying the Role of Orbital Contraction in Chemical Bonding. *J. Phys. Chem. Lett.* **2017**, *8*, 1967–1972.

(27) Levine, D. S.; Head-Gordon, M. Energy decomposition analysis of single bonds within Kohn–Sham density functional theory. *Proc. Nat. Acad. Sci.* **2017**, *114*, 12649–12656.

(28) Hiberty, P. C.; Ramozzi, R.; Song, L.; Wu, W.; Shaik, S. The physical origin of large covalent-ionic resonance energies in some two-electron bonds. *Faraday Discuss.* **2007**, *135*, 261–272.

(29) Horn, P. R.; Head-Gordon, M. Polarization contributions to intermolecular interactions revisited with fragment electric-field response functions. *J. Chem. Phys.* **2015**, *143*, 114111.

(30) West, A. C.; Schmidt, M. W.; Gordon, M. S.; Ruedenberg, K. A Comprehensive Analysis in Terms of Molecule-Intrinsic, Quasi-Atomic Orbitals. II. Strongly Correlated MCSCF Wave Functions. *J. Phys. Chem. A* **2015**, *119*, 10360–10367.

(31) West, A. C.; Schmidt, M. W.; Gordon, M. S.; Ruedenberg, K. A Comprehensive Analysis in Terms of Molecule-Intrinsic, Quasi-Atomic Orbitals. III. the Covalent Bonding Structure of Urea. *J. Phys. Chem. A* **2015**, *119*, 10368–10375.

(32) West, A. C.; Schmidt, M. W.; Gordon, M. S.; Ruedenberg, K. A Comprehensive Analysis in Terms of Molecule-Intrinsic Quasi-Atomic Orbitals. IV. Bond Breaking and Bond Forming along the Dissociative Reaction Path of Dioxetane. *J. Phys. Chem. A* **2015**, *119*, 10376–10389.

(33) West, A. C.; Schmidt, M. W.; Gordon, M. S.; Ruedenberg, K. Intrinsic Resolution of Molecular Electronic Wave Functions and Energies in Terms of Quasi-atoms and Their Interactions. *J. Phys. Chem. A* **2017**, *121*, 1086–1105.

(34) West, A. C.; Duchimaza-Heredia, J. J.; Gordon, M. S.; Ruedenberg, K. Identification and Characterization of Molecular Bonding Structures by ab initio Quasi-Atomic Orbital Analyses. *J. Phys. Chem. A* **2017**, *121*, 8884–8898.

(35) Duchimaza Heredia, J. J.; Ruedenberg, K.; Gordon, M. S. Quasi-Atomic Bonding Analysis of Xe-Containing Compounds. *J. Phys. Chem. A* **2018**, *122*, 3442–3454.

(36) Duchimaza Heredia, J. J.; Sadow, A. D.; Gordon, M. S. A Quasi-Atomic Analysis of Three-Center Two-Electron Zr-H-Si Interactions. *J. Phys. Chem. A* **2018**, *122*, 9653–9669.

(37) Schoendorff, G.; Schmidt, M. W.; Ruedenberg, K.; Gordon, M. S. Quasi-Atomic Bond Analyses in the Sixth Period: II. Bond Analyses of Cerium Oxides. *J. Phys. Chem. A* **2019**, *123*, 5249–5256.

(38) Guidez, E. B.; Gordon, M. S.; Ruedenberg, K. Why is Si2H2Not Linear? An Intrinsic Quasi-Atomic Bonding Analysis. *J. Am. Chem. Soc.* **2020**, *142*, 13729–13742.

(39) Schoendorff, G.; Ruedenberg, K.; Gordon, M. S. Multiple Bonding in Rhodium Monoboride. Quasi-atomic Analyses of the Ground and Low-Lying Excited States. *J. Phys. Chem. A* **2021**, *125*, 4836–4846.

(40) Epifanovsky, E. et al. Software for the frontiers of quantum chemistry: An overview of developments in the Q-Chem 5 package. *J. Chem. Phys.* **2021**, *155*, 084801.

(41) Dunning, T. H. Gaussian basis sets for use in correlated molecular calculations. I. The atoms boron through neon and hydrogen. *J. Chem. Phys.* **1989**, *90*, 1007–1023.

(42) Mardirossian, N.; Head-Gordon, M. ωB97M-V: A combinatorially optimized, range-separated hybrid, meta-GGA density functional with VV10 nonlocal correlation. *J. Chem. Phys.* **2016**, *144*, 214110.

(43) Luo, Y.-R. *Comprehensive Handbook of Chemical Bond Energies*, 1st ed.; CRC Press, 2007.

(44) Kaupp, M. The role of radial nodes of atomic orbitals for chemical bonding and the periodic table. *J. Comput. Chem.* **2007**, *28*, 320–325.

(45) Wang, Z.-L.; Hu, H.-S.; von Szentpály, L.; Stoll, H.; Fritzsche, S.; Pyykkö, P.; Schwarz, W. E.; Li, J. Understanding the uniqueness of 2p elements in periodic tables. *Chem. Eur. J.* **2020**, *26*, 15558–15564.

(46) Danovich, D.; Wu, W.; Shaik, S. No-pair bonding in the high, spin $3\Sigma(u)/+$ state of Li2. A valence bond study of its origins. *J. Am. Chem. Soc.* **1999**, *121*, 3165–3174.

(47) Harrison, J. F.; Lawson, D. B. Some observations on molecular orbital theory. *J. Chem. Educ.* **2005**, *82*, 1205–1209.

(48) Müller, W.; Jungen, M. Excited states of Li2+. *Chem. Phys. Lett.* **1976**, *40*, 199–204.

(49) Shaik, S.; Danovich, D.; Galbraith, J. M.; Braïda, B.; Wu, W.; Hiberty, P. C. Charge-Shift Bonding: A New and Unique Form of Bonding. *Angew. Chem. Int. Ed.* **2020**, *59*, 984–1001.

(50) Sanderson, R. T. *Polar Covalence*; Academic Press: New York, 1983.

(51) Hirshfeld, F. L.; Rzotkiewicz, S. Electrostatic binding in the first-row AH and A2 diatomic molecules. *Mol. Phys.* **1974**, *27*, 1319–1343.

(52) Allred, A. L. Electronegativity values from thermochemical data. *J. Inorg. Nucl. Chem.* **1961**, *17*, 215–221.

(53) Knizia, G. Intrinsic atomic orbitals: An unbiased bridge between quantum theory and chemical concepts. *J. Chem. Theory Comput.* **2013**, *9*, 4834–4843.

(54) Spackman, M. A.; Maslen, E. N. Chemical properties from the promolecule. *J. Phys. Chem.* **1986**, *90*, 2020–2027.

(55) Mó, O.; Yáñez, M.; Eckert-Maksić, M.; Maksić, Z. B.; Alkorta, I.; Elguero, J. Periodic trends in bond dissociation energies. A theoretical study. *J. Phys. Chem. A* **2005**, *109*, 4359–4365.

(56) Blokker, E.; Sun, X.; Poater, J.; van der Schuur, J. M.; Hamlin, T. A.; Bickelhaupt, F. M. The Chemical Bond: When Atom Size Instead of Electronegativity Difference Determines Trend in Bond Strength. *Chem. Eur. J.* **2021**, *27*, 15616–15622.

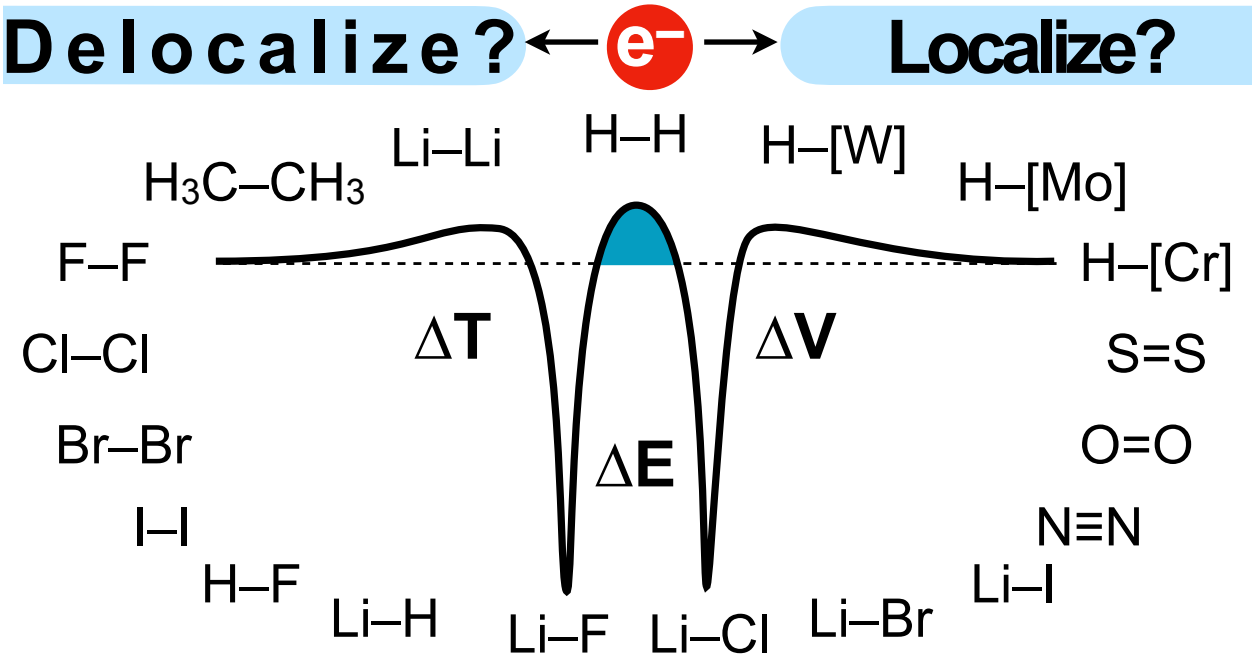

Figure 10: TOC Graphic